Aging Mechanism and Life Estimation of Photovoltaic Inverter DC-link Capacitors in Alternating Humid and Thermal Environment*

Quanyi Gao[1], *Shuaibing Li*[1, 2*], *Yi Cui*[3], *Yongqiang Kang*[1, 2] *and Haiying Dong*[1]

(1. School of New Energy and Power Engineering, Lanzhou Jiaotong University, Lanzhou 730070, China;
2. State Key Laboratory of Large Electric Drive System and Equipment Technology, Tianshui 741000, China;
3. School of Engineering, University of Southern Queensland, Springfield 4300, Australia)

Abstract: DC-link capacitors play a vital role in managing ripple voltage and current in converters and various devices. This study focuses on exploring the aging characteristics of DC-link capacitors in alternating humid and thermal environments aligned with the operational conditions in photovoltaic and wind power applications. Adhering to relevant power equipment standards, we designed a 24-h alternating humid and thermal aging environment tailored to the requirements of DC-link capacitors. An aging test platform is established, and 20 widely used metallized polypropylene film capacitors are selected for evaluation. Parameters such as the capacitance, equivalent series resistance (ESR), and phase angle are assessed during aging, as well as the onset time and extent of aging at various intervals. This study focuses on the aging mechanisms, analyzing electrode corrosion, the self-healing process, and dielectric aging. Fitting the aging characteristics enabled us to calculate the lifespan of the capacitor and predict it under different degrees of capacitance decay. The results show that under alternating humid and thermal conditions, capacitance attenuation and ESR increase exhibit exponential nonlinearity, influenced by factors such as the oxidation and self-healing of capacitive metal electrodes, dielectric main-chain fracture, and crystal transformation. This study underscores the pivotal role of encapsulation in determining the aging decay time.

Keywords: DC-link capacitors, aging mechanism, life prediction, metallized film capacitors

1 Introduction

In the context of the global drive for carbon neutrality, photovoltaic (PV) power generation has emerged as a critical component of clean energy production and the development of smart grids [1-2]. With the robust growth in PV power generation, PV converters encounter increasingly intricate grid-connected conditions and challenging geographical environments [3]. The DC-link capacitor is responsible for stabilizing the DC voltage, absorbing high- and low-frequency ripple currents, and balancing the power differential between the two sides. In reliability research on power electronic equipment, the vulnerability of DC-link capacitors ranks second [4]. Confronted with the high temperatures and humidity prevalent in beach and offshore working environments, they undergo accelerated aging, decreasing the capacitor capacity. This decline has a significant impact on inverter control and stability.

In the exploration of capacitor aging, numerous scholars have investigated the impact of single or combined factors on capacitor aging, focusing on the three primary factors that affect capacitors: voltage levels, temperature, and humidity [5]. When examining capacitor aging influenced by temperature alone, the degree of aging varies across temperatures ranging from 40 ℃ to 180 ℃. Structural changes before and after capacitor aging have been observed using different electron microscopes [6]. Aging tests were conducted on 34 metallized film capacitors under the combined influence of voltage and temperature at different voltage and temperature settings. The capacitive aging function over time has been derived using the exponential probability rule, and parameter fitting and

Manuscript received November 27, 2023; revised January 24, 2024; accepted February 20, 2024. Date of publication March 31, 2024; date of current version February 28, 2024.
* Corresponding Author, E-mail: lishuaibing1105@163.com
* Supported by the Opening Project of State Key Laboratory of Large Electric Drive System and Equipment Technology (SKLLDJ022020004).
Digital Object Identifier: 10.23919/CJEE.2024.000054

extrapolation were performed at various voltages and temperatures [7]. To address the combined aging of AC metallized capacitors owing to temperature, humidity, and voltage, high temperature and high humidity, both at the rated AC voltage, were simultaneously applied to two AC magnetic suppression capacitors with different aluminum contents in the metallized film. Curves that depict the capacitance attenuation and ESR growth characteristics were obtained [8]. Subsequently, water intrusion under different humidity conditions at high temperatures was examined, yielding capacitance attenuation characteristic curves under various humidity conditions. Water intrusion was gauged by the weight increase [9]. Building on prior studies on water intrusion at different humidity levels, the morphologies of the metallized films and electrodes were observed at different magnifications [10]. Regarding the aging of DC capacitors, the capacitance attenuation and ESR growth characteristics of the metallized DC film capacitor were fitted under the joint influence of the ripple voltage, high-temperature (85 ℃), and varying humidity. The analysis revealed differences in performance at different humidity levels under high-temperature conditions [11].

Studies on the aging mechanism of thin-film capacitors initially focused on voltage and temperature, yielding significant accomplishments. Subsequently, the introduction of humidity as an influencing factor enhanced our understanding of capacitor aging. In the investigation of the aging mechanism of dielectric films, low temperature oxygen induces an increase in the crosslinking density, whereas high-temperature oxygen reduced residue formation. Elevated oxide levels obstruct the oxygen infiltration path, thereby slowing thermal degradation [12]. As the temperature rises, main chain breaks occur, polarized free radicals increase, shallow trap density increases, the activation energy of molecular chain segment motion decreases, and crystallinity decreases. This reduces the breakdown time of the film and increases its dielectric conductivity [13-17]. Electrochemical corrosion of the polymer surface originates from the oxygen and water absorbed within the medium and is dependent on the temperature, voltage, and frequency. Electrochemical corrosion, under the influence of an electric field and water, causes simultaneous corrosion at multiple positions on the electrode. During electrochemical corrosion, electrode oxidation accelerates capacitor decay [18-20]. The moisture entry time is determined by the packaging, with temperature playing a key role. In addition to temperature, humidity, voltage, and radiation can also contribute to the aging of metallized polypropylene film capacitors. Following radiation crosslinking, polypropylene absorbs radiation energy, resulting in the breaking of C—H bonds in the main molecular chain, forming free radicals. The carbon atoms of the free radicals then form crosslinked bonds, resulting in cross-linked products [21].

Most of the research discussed above pertains to metallized film capacitors utilized in AC applications, with a notable absence of aging characteristics for DC-link capacitors used in PV converters. Moreover, all aging tests for capacitors thus far have considered a fixed combination of temperature, humidity, and voltage, which deviates from the actual working environment of DC-link capacitors in PV converters. Consequently, the obtained aging characteristics may not be applicable.

Considering a real environment, this study investigates the aging characteristics and mechanisms of DC-link capacitors by proposing an alternating humid and thermal aging environment tailored to the specific needs of DC-link capacitors. The second chapter introduces the fundamental structure of metallized film capacitors, describes the design of an alternating humid and thermal environment that aligns with the actual working conditions of DC-link capacitors, and establishes an aging test platform. In the third chapter, the capacitor aging characteristics are analyzed through changes in capacitance, ESR, and phase angle over time. Aging mechanisms are examined from three perspectives: electrode corrosion, self-healing, and dielectric aging. The fourth chapter predicts the lifespan under different levels of capacity attenuation through data fitting of aging characteristics. Finally, the fifth chapter presents the conclusions.

2 Alternating humid and thermal aging test of metallized capacitors

2.1 Aging test setup

2.1.1 Alternating humid and thermal environment

In tidal flats and offshore areas, humidity remains

consistently high, and a the temperature difference between the day and night is high. During daylight hours, when lighting conditions are ample, the ambient temperature outside a PV converter can exceed 60 ℃ and reach 75 ℃. Owing to the inherent heating of the PV converter and other power electronic equipment, the temperature near the internal capacitor is even higher. At night, temperatures rapidly decrease, maintaining a range of 0 ℃ to 10 ℃. To replicate the alternating humid and thermal environment experienced by DC-link capacitors within a day under these conditions, we designed a 24 h alternating humid and thermal aging cycle, as illustrated in Fig. 1. The design draws references from standards such as GJB 360B-2009, GB/T 2423.4-2016, and IEC 60068-2-30 [22-24]. Fig. 1 depicts the temperature variations over time: in the initial 16 h, the temperature rises and cools twice, fluctuating between 25 ℃ and 85 ℃. During this period, the high-temperature of 85 ℃ is maintained for 6 h, followed by a one-hour maintenance at 25 ℃. Subsequently, there is a rapid cooling by –10 ℃ within 15 min, maintained for 3 h, followed by a gradual return to 25 ℃ over the next 45 min until the end. The inclusion of low temperatures simulates the night-time working environment of DC-link capacitors and accelerates humidity intrusion. Fig. 1 illustrates that the humidity was consistently maintained at 93%RH and remained uncontrolled at low temperatures. This deliberate lack of humidity control at low temperatures enhances the humidity intrusion. The repeated condensation and respiration induced by temperature cycling under high-humidity conditions intensified humidity intrusion and prolonged the duration of water remaining inside the DC-link capacitor.

2.1.2 Experimental setup

This study utilizes a programmable constant temperature and humidity chamber to establish precise and stable alternating humidity and thermal conditions for DC-link capacitors. The temperature range of the chamber spans from –40 ℃ to 150 ℃, while the humidity range is set between 20% and 98% relative humidity (RH). The heating rate is adjustable between 2 ℃ and 4 ℃ per minute, and the cooling rate ranges from 0.7 ℃ to 1 ℃ per minute. The programmable chamber offers a rapid response in maintaining a set temperature and humidity, closely simulating the significant temperature variations and high-humidity conditions encountered by DC-link capacitors during operation. To facilitate the application of voltage stress to the DC-link capacitor, energized terminals are incorporated into the side walls of the chamber. Additionally, a programmable DC voltage source is employed to apply DC voltage to the DC-link capacitor. The power capacity of the programmable DC voltage source is 2.5 kW, enabling the provision of a 50-750 V DC voltage. This setup enables the application of electrical stress to a DC-link capacitor, mimicking real-world working conditions.

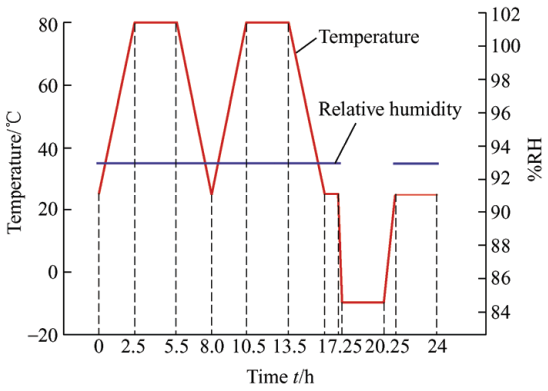

Fig. 1 Designed alternating humid and thermal aging condition

2.2 Experimental apparatus and system

2.2.1 Metallized film capacitors

The common structure of a metallized film capacitor (MFC) is wound, as illustrated in Fig. 2. The typical configuration involves the deposition of nano-sized aluminum, zinc, or their alloys onto a micron-thick polymer film via a physical vapor deposition (PVD) process conducted under vacuum conditions. Two layers of the metallized polymer film are superimposed and wound around a polyurethane mandrel [25]. Metal terminals are drawn through the “Schoopage” spray end and inserted into a plastic housing along with the winding structure. The entire assembly is infused with epoxy material to firmly fix the MFC, rendering it moisture proof and flame retardant. A profile structure diagram of the MFC is shown in Fig. 3. To fulfill the insulation protection requirements, a certain blank is left at one end of the metallized film, and the metallized film at the other

end is thickened. This is known as the heavy edge (HE) process [26-27]. The implementation of the HE process enhances the contact between metal particles sprayed onto the metallized electrode using "Schoopage" technology. Moreover, the heat dissipation resulting from the reduced resistivity at the HE helps mitigate the contraction and disconnection of the metallized film at the contact edge [28].

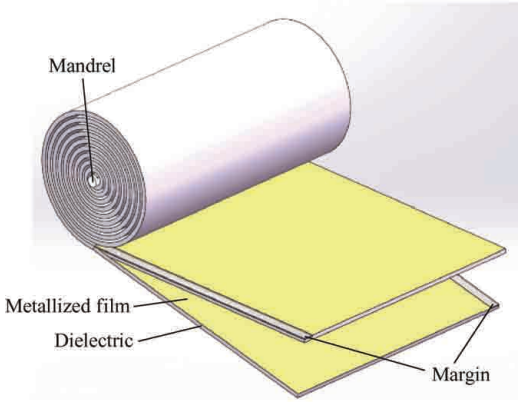

Fig. 2 Structure of MFC

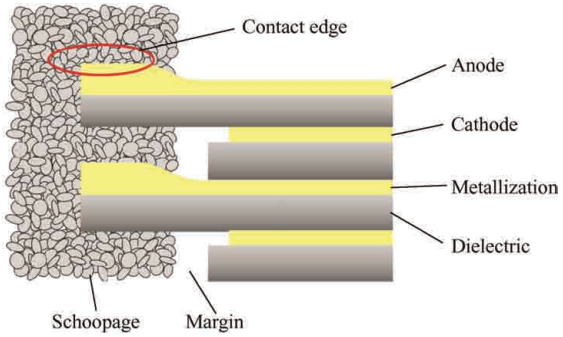

Fig. 3 Schematic of MFC profile structure

In this study, DC-link metallized polypropylene film capacitors obtained from Xiamen Fara Electronics and American Kemet were chosen for the aging experiments, with each brand constituting a separate group. Each group comprised ten capacitors, labeled C10 to C19 for the Xiamen Fara Electronics group (Group 1) and C20 to C29 for the American Kemet group (Group 2). The technical parameters of the two capacitor sets are listed in Tab. 1. Both capacitors feature rectangular plastic housing designs. The winding structure, as depicted in Fig. 1, is sealed with epoxy filling, and the two pins closer together are linked to the "Schoopage" coating on one side. As illustrated in Fig. 4, Group 2 exhibits a larger volume than Group 1. When the two capacitor winding structures are similar in size, Group 2 has a larger proportion of filled resin packages.

Tab. 1 Selected capacitor technology parameters

Technical data	Group 1	Group 2
Capacitance C_{10}-C_{29}/μF	100	100
Rated voltage U_N/V	600	800
dv/dt/(V/μs)	15	9
ESR @10 kHz/mΩ	4.2	2.2
I_{max}/A	28.7	40.6
tanδ/×10^{-4}	36	20
T_{rated}/℃	85	85
T_{max}/℃	105	125
T_{min}/℃	–50	–55
Capacitance tolerance(%)	±5	±5
Life expectancy$_{85℃}$/h	35 000	100 000

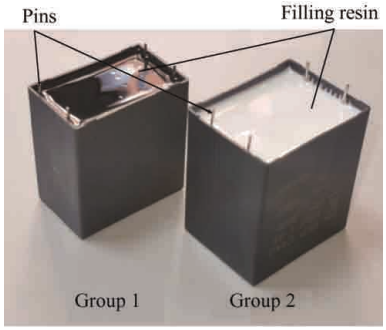

(a) Physical diagram of capacitor before aging

(b) Physical diagram of capacitor after aging

Fig. 4 Physical diagram of the capacitor before and after alternating humidity and thermal aging

2.2.2 Alternating humid and thermal aging system

A schematic of the designed experimental system and the configuration of the alternating humid and thermal aging platforms are shown in Fig. 5. To limit the volume of the test oven, 20 metallized polypropylene film capacitors were used for testing. The capacitors, separated to groups 1 and 2, are connected in parallel with the buffer resistor R. This configuration ensures that the pulse current passing through the experimental capacitors does not exceed the maximum current that they could withstand, thereby preventing breakdown. The simplified circuit of the programmable DC voltage source comprises an ideal voltage source, switch K1, and a controller with a sensor and a circuit breaker. Operation ceases when the circuit breaker is

disconnected. When K_1 is closed and K2 is disconnected, a DC voltage is applied to both ends of the 20 metallized polypropylene film capacitors. Switch K1 is disconnected at the end of each 24 h alternating humid and heat aging cycle, and K2 is closed to complete the discharge of the capacitors.

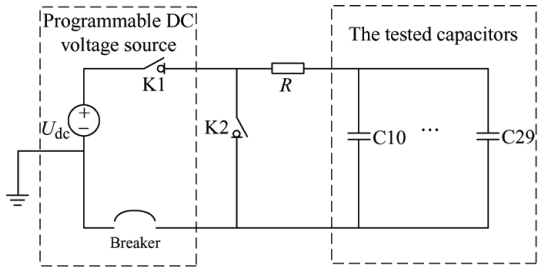

(a) Schematic diagram of the designed experimental system

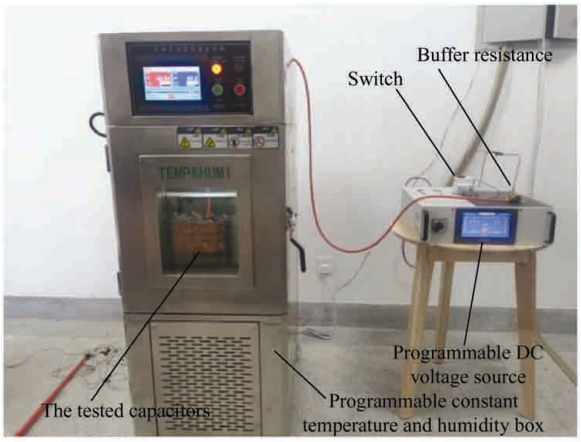

(b) Alternating humid and thermal aging platform

Fig. 5 Experimental platform for alternating humid and thermal aging

In the experimental platform for alternating humid and thermal aging, the programmable DC voltage source supplies a 600 V DC voltage to the 20 capacitors through a high-voltage insulated wire, which enters the side energized connection port designed to withstand high temperatures and high humidity. The programmable constant temperature and humidity box ensures precise alternating humidity and thermal conditions. The three influencing factors—voltage, humidity, and temperature—act in combination on the 20 DC-link capacitors in a 24 h cycle. The capacitance and ESR of the capacitors are measured after each cycle. The normalized changes in capacitance and ESR are defined as follows

$$\Delta C = \frac{C(t) - C_0}{C_0} \times 100\% \tag{1}$$

$$\Delta \mathrm{ESR} = \frac{\mathrm{ESR}(t)}{\mathrm{ESR}_0} \times 100\% \tag{2}$$

3 Aging experiment results and analysis

This study focuses on explaining the changes in the overall state of capacitors from a macro perspective rather than from a micro perspective. Thus, the ESR and changes in capacitance values are used to reflect the aging of the capacitors.

3.1 Capacity change

Fig. 6 illustrates the normalized capacitance decay over time for the Group 1 capacitors (excluding C18). It is evident that for the initial 800 h, the capacitance remains unchanged. This period corresponds to the intrusion of water. C13, C14, C15, and C17 exhibit the earliest capacitance change of –0.1% at 816 h, while C12 and C19 show the latest capacitance change of –0.1% at 888 h, with the residual capacitance adjusting correspondingly at 840 h. Generally, metallized film capacitors tend to exhibit a capacity attenuation of –5%, considered indicative of reaching the end of their life. C15 shows a capacity attenuation of more than 5% at 1 632 h, C13 and C17 at 1 680 h, C10, C11, and C14 at approximately 1 752 h, and C12 and C16 manifested later at 1 824 h and 1 896 h, respectively. At the conclusion of the aging experiment at 2 232 h, the capacitance attenuation of C19 is only –4.66%, whereas the capacitance changes of C10, C13, C15, and C17 are –11.52%, –11.80%, –11.96%, and –11.45%, respectively.

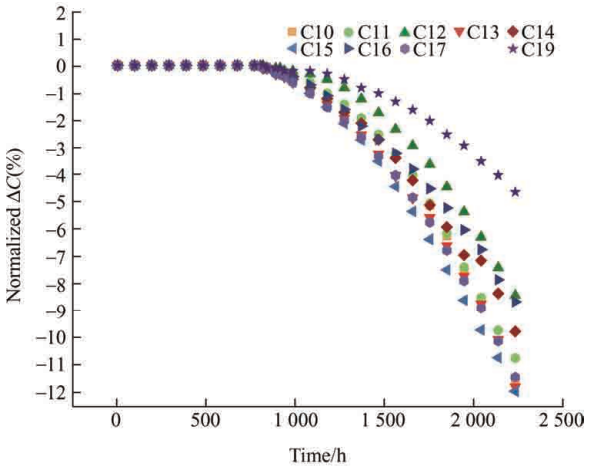

Fig. 6 Group 1 (except C18) normalized capacitance changes

The capacitance decay trend of C19 closely aligns with those of the other eight capacitors; however, its degree of aging is significantly lower. At 1 752 h, it

experiences only a –2.03% attenuation, which is less than half of the attenuation observed in the other capacitors. Several factors contribute to this phenomenon. First, although the materials and manufacturing processes are the same, the materials used to manufacture the capacitor may originate from different batches or suppliers. Even if they share nominal specifications, slight variations in the materials, particularly in thin-film dielectric polymers, may occur between batches. Second, environmental conditions during the manufacturing process and operational periods, such as equipment temperature and humidity, can affect the tensile properties of the capacitive insulating polymer, roughness of the metallized film layer, and the adhesion tightness of the "Schoopage" spray layer to the metal electrode. Third, the order and positions of the capacitors were fixed for each experiment. Although efforts were made to control the uniformity of temperature and humidity during the experiment, the limitations of the experimental equipment, such as the proximity of the capacitor to the outer wall of the inner cabin and contact overlap with adjacent capacitor shells, can hinder the uniformity of humidity and water intrusion to some extent.

C18 exhibits a capacity attenuation of –0.1% at 840 h and –3.77% at 1 560 h. Subsequently, there exists a sharp decrease in the tolerance value, reaching –20.98% at 1 656 h and further declining to –49.09% at 1 752 h. Over the subsequent 480 h, the capacity value of C18 experiences minimal significant changes, and by 2 232 h, the capacity value decreases to –49.36%, as illustrated in Fig. 7.

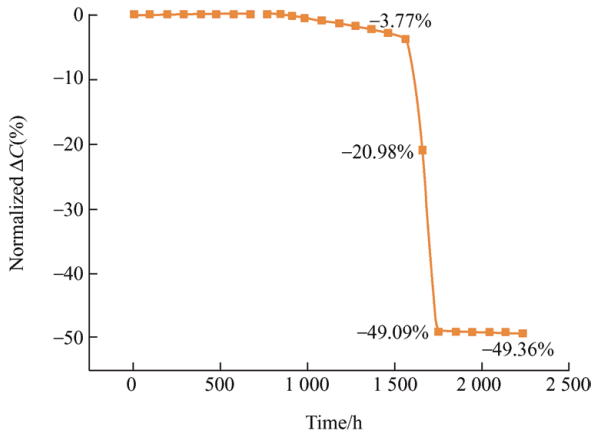

Fig. 7 C18 normalized capacitance changes

Under the combined impact of high humidity and significant temperature variations during alternating humidity and thermal cycles, the plastic shells of the C18 develops cracks, consequently damaging the epoxy resin package. The winding structure of the silver-white metallized polypropylene film is prominently exposed to the external environment and makes direct contact with it, as shown in Fig. 4. The abrupt decrease in the capacitance of C18 from 1 656 h to 1 752 h can be attributed to water directly infiltrating the capacitor through gaps in the high-humidity environment. This intrusion causes local breakdown of the positive and negative electrodes, releasing a substantial amount of energy. The electric polarization ability of the partially penetrated polypropylene medium is significantly reduced, and the released energy causes volatilization of the metallized film. Consequently, the effective area of the metallized electrode film diminishes, leading to a sharp reduction in the capacitance. After 1 752 h, the capacitance remains nearly unchanged, with only minor capacitance attenuation. Owing to the favorable self-healing property of the metallized polypropylene film capacitors, the winding structure near the gap self-heals, blocking the intrusion of humidity. It is anticipated that the capacitor will resume the aging decay process when the humidity completely traverses the self-healing metallized polypropylene film and no further breakdown occurs

In Group 2, it took approximately 900 h for the moisture to infiltrate the epoxy package, as shown in Fig. 8. The capacitance of C22 and C29 initially changed by –0.1% at 912 h, with the residual capacitance

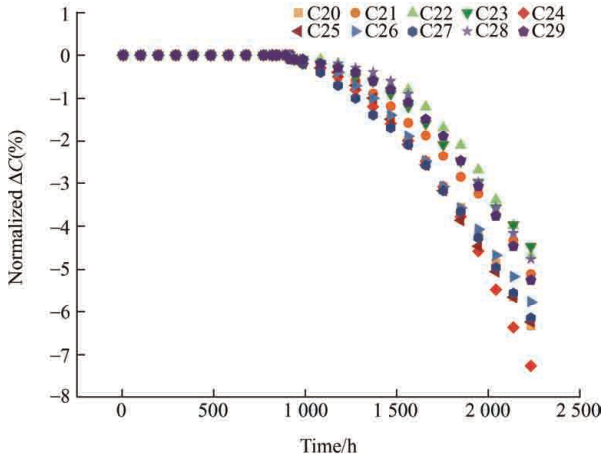

Fig. 8 Normalized capacitance changes in Group 2

adjusting correspondingly at 936 h. At the conclusion of the experiment, the capacity attenuation of C23 is the smallest at –4.48%, while the capacity attenuation of C24, at –7.28%, is the largest. In addition to C22 and C23, eight capacitors exhibit a capacity attenuation of more than 5%.

3.2 Equivalent series resistance change

In the temporal evolution of the normalized ESR for Group 1, an overall nonlinear growth trend is observed, except for the other nine capacitors represented by C18. At 888 h, the ESR of C14, C17, and C18 increases by 5%, whereas the ESR of C13 simultaneously increases by 10%. Corresponding changes in the remaining capacitance occur after 912 h, as illustrated in Fig. 9. Generally, a normalized ESR exceeding 3 is indicative of the end of a metallized film capacitor lifespan [29]. By 1 944 h, ΔESR of C10, C11, C13, C15, and C16 surpassed 3, with the remaining capacitance following suit around 2 100 h. Notably, the ESR of C18 rises to 1.45 at 1 560 h. However, owing to direct contact between the internal winding structure and the highly humid external environment resulting from damage to the shell and packaging, a short conductive channel forms after the breakdown of the polypropylene film medium. The measured ESR sharply drops to 0.65 at approximately 1 700 h. Upon completion of self-healing, the ESR of the C18 capacitor returns to 0.65 and gradually recovers to its initial value.

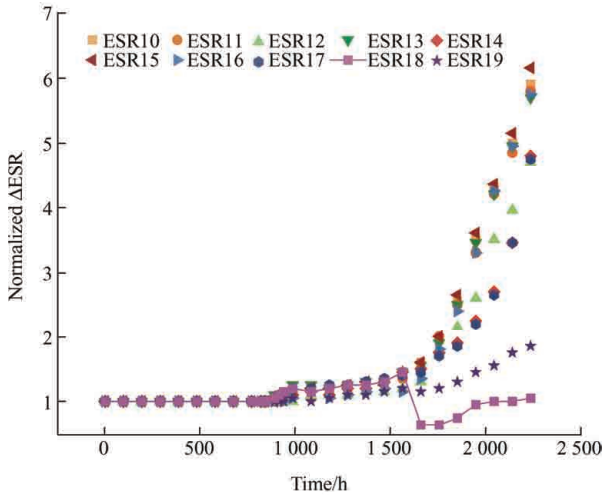

Fig. 9 Group 1 normalized ESR changes

The increase in Group 2 was significantly smaller than that in Group 1. C20, C25, and C29 initially experienced a 1.05 increase at 984 h, with C22 showing a corresponding increase by 1 272 h, and the residual capacitance changing accordingly at 1 100 h. By the end of the experiment, C20, C24, C24, and C27 exceeded 3, while the remaining capacitance remained at approximately 2. C23 exhibits the smallest growth at 1.9, whereas C20 exhibits the largest growth at 3.6, as illustrated in Fig. 10.

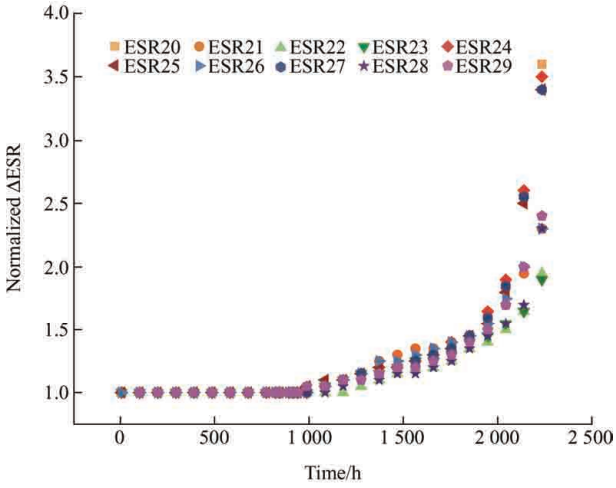

Fig. 10 Group 2 normalized ESR changes

3.3 Phase angle change

Owing to inevitable ESR and medium loss, the initial phase angle of both Group 1 and Group 2 is approximately –83.1°. As shown in Fig. 11, after alternating humid and thermal aging, the minimum phase angle change for Group 1 (excluding C18) is 16.1°, maximum phase angle change is 27°, and average phase angle change is 23°. However, the absolute phase angle of C18 increased by 1.3° because of the breakdown caused by the direct contact between the internal winding structure and the highly humid external environment. The damaged polypropylene winding formed protected the undamaged internal winding after the completion of self-healing. Group 2 exhibits a minimum phase angle change of 6.5°, maximum phase angle change of 14.2°, and an average phase angle change of 10.7°.

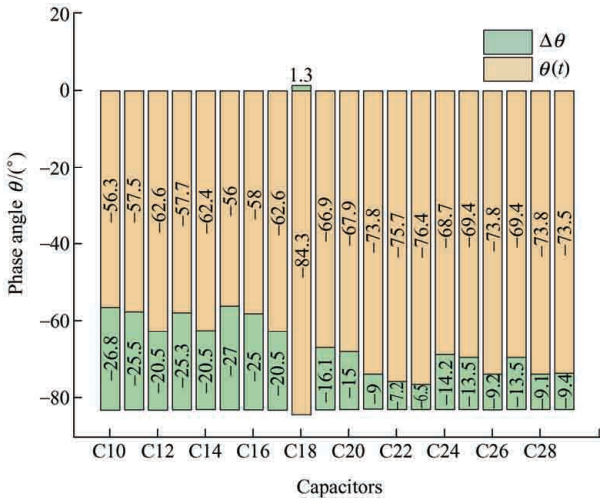

Fig. 11 Phase angle changes in Groups 1 and 2

3.4 Aging mechanism analysis

The aging of metallized polypropylene film capacitors is primarily influenced by electrode corrosion, the self-healing process, and the aging of the polypropylene film medium. Electrode corrosion and the self-healing process have a notable impact on capacitance attenuation, while aging of the polypropylene film medium contributes to capacitor enlargement, increasing energy loss, and an elevated temperature rise inside the capacitor, consequently affects the life and reliability of the capacitor.

3.4.1 Electrode corrosion

A metallized electrode on the polymer film of a metallized capacitor is typically fabricated by depositing aluminum, zinc, or different proportions of the two alloys. Despite efforts to minimize oxygen exposure in the vacuum during the manufacturing process, realistic conditions result in the inevitable entry of oxygen into the winding structure and resin packaging. Consequently, a small amount of oxygen is already present inside the capacitor during manufacturing. The ionization energy of aluminum and zinc accurately reflects the ability of the metal to gain and lose electrons, indicating its reactivity. The first ionization energies of aluminum and zinc are 577 kJ/mol and 906 kJ/mol, respectively, signifying that aluminum exhibits stronger reducibility than zinc and is more prone to react with oxygen. The reactions between Al, Zn, and oxygen are shown in Eqs. (3) and (4) and Eqs. (5) and (6) describe the reactions of Zn with water and oxygen. Eqs. (3) and (4) readily occur at room temperature, and the high-temperature process promotes Eqs. (5) and (6), respectively. Simultaneously, the low-temperature plunge under alternating humid and thermal conditions prolongs the water retention time inside the capacitor, further catalyzing the reaction between water and oxygen with the metallized film electrode. The process occurs at both the positive and negative electrodes, with Al_2O_3 and ZnO acting as insulators that impede electron conduction to a certain extent.

$$4Al + 3O_2 \rightarrow 2Al_2O_3 \tag{3}$$

$$2Zn + O_2 \rightarrow 2ZnO \tag{4}$$

$$Zn + 2H_2O \rightarrow Zn(OH)_2 + H_2\uparrow \tag{5}$$

$$2Zn + O_2 + 2H_2O \rightarrow 2Zn(OH)_2 \tag{6}$$

Mott and Cabrera elucidated the formation of a thin oxide layer using a double electric layer model and investigated the growth patterns of the oxide layer within 100 nm of the metal [30]. Under alternating humid and thermal conditions, water molecules adhere to the electrode surface, and the oxygen molecules within the water approach the interface between the oxide and water. They then combine with the electrons from the oxide to form a negative plate. This negative charge attracts metal cations near the interface, resulting in the formation of a positive plate. Positive and negative plates drive the combination of metal cations and oxygen ions under the influence of a strong electric field. The specific reaction process is illustrated in Fig. 12 [19]. Over time, the electrode thickness of the MFC decreases, increasing the roughness of the capacitive metal electrode. This uneven enhancement of the dielectric uniformity contributes to the attenuation of the capacitance.

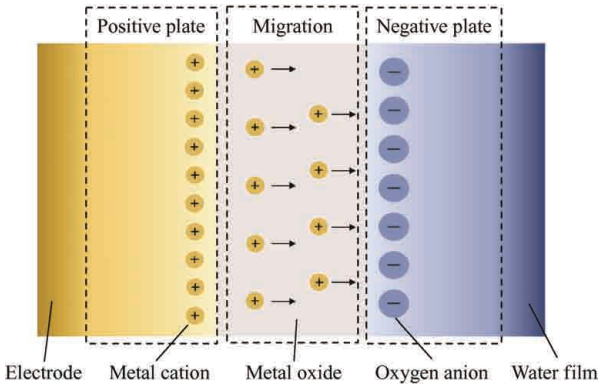

Fig. 12 Double electric layer model of thin-film attenuation of the metal electrode

3.4.2 Self-healing process

Although the metallized electrode of MFC is designed for smoothness during processing and manufacturing, the inherent process level necessitates a certain roughness on its surface, including the presence of burrs and spikes in the metal layer. Additionally, the impact of electrode corrosion exacerbates the uneven surface of the metallized electrode, affecting the polypropylene and other dielectric films, as well as the interface between them. This results in an irregular distribution of interfacial electric fields and a concentration of space charges when a voltage is applied [31]. Under the influence of high temperature, humidity, and pressure, partial discharge occurs at the interface because of impurities, defects, and gas gaps in the dielectric film [32]. A localized breakdown occurs when the local part of the medium exceeds the maximum voltage it can withstand, and the substantial energy generated instantaneously causes the local metallized electrode film layer on the surface of the medium to volatilize. Part of the medium melts and returns to a solid state after cooling, while another part becomes electrically isolated. This constitutes the self-healing process of the MFC, as shown in Fig. 13 [33]. Self-healing reduces the failure rate of MFC, enhances their stability, and extends their service life. However, a reduction in the area of the effective metallized film and dielectrics, whose chemical properties change after local breakdown, also decreases the capacitance and increases the dielectric loss. Furthermore, the self-healing process and microbubbles generated by electrode corrosion increase the pressure inside the capacitor, thus increasing the risk of damage to the wound structure, resin packaging, and housing [34].

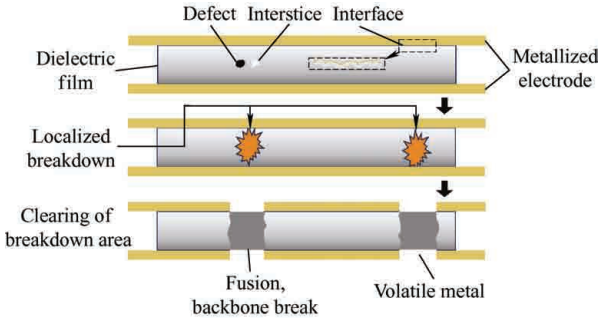

Fig. 13 Self-healing process of the MFC

3.4.3 Dielectric aging

Alterations in the basic structure and surface morphology of dielectric films are the primary determinants of the film performance [35]. Prolonged aging of the medium is primarily attributed to physical and chemical structural changes in the polymer material under specific conditions such as voltage, temperature, and humidity. Medium degradation signifies a substantial alteration in the chemical properties of a polymer, resulting in significant and undesirable changes in its intrinsic characteristics. The variation in dielectric loss effectively reflects the aging conditions of the medium. In addition to the external conditions, impurities, residual catalysts, and antioxidants within the medium have the potential to contribute to medium loss.

Polypropylene crystals exist in three forms: monoclinic α, hexagonal β, and orthogonal crystallization γ, where the single crystal α indicates the predominant structure, and the latter two are formed under shear and high pressure, respectively [35]. A polypropylene film comprises a crystalline phase with high stress, an amorphous phase lacking long-range or local order, and a rigid amorphous phase with a disordered transition between them [36]. The crystalline and amorphous zones are sized 10 nm, and the size of the interface zone is 1 nm. The transformation of $\beta \rightarrow \alpha$ initiates when the cast film is heated to the tensile temperature [37]. During the tensile process of the polypropylene film, the rotation and separation of the lamellae lead to the formation of micropores in the amorphous phase between the lamellae. Beyond the yield point, these initial holes evolve into larger ones, completing the transformation from β to α and resulting in stress-induced lamellar rupture [35]. When these holes are subjected to increased internal pressure and tensile stress, fine cracks form because of the stress concentration caused by defects, cracks, and inhomogeneity [38]. Thermal aging exacerbates the development of fine cracks, particularly owing to respiration caused by alternating humid and thermal conditions. This results in breakage of the polymer main chain, reduction of molecular length and mechanical strength, and an increase in partial discharge, elevating the risk of breakdown [39].

Fig. 14 depicts the molecular structure of

polypropylene [40]. During thermal aging and oxidation, polypropylene molecules impart excessive energy to the main chain, resulting in the breakdown and decomposition of the main chain and the formation of peroxides, carbonyl groups, branched carbon chains, and unsaturated structures. Fig. 15 illustrates that the three unsaturated types displayed after the main-chain fracture lead to the formation of a single double bond [41]. The strength of these free radicals surpasses that of the main chain, promoting oxidation and increasing main-chain breakage, and the short chains formed during continuous decomposition enhance the orientation polarization and foster film degradation. In addition to thermal aging, space charge injection and accumulation caused by the electric field action induce local electric field distortion in the medium. The resulting electromechanical stress deforms the molecular chains and contributes to material aging [42]. Impurities and defects in the medium have varying abilities to attract charge carriers, which can be categorized into shallow and deep traps. Owing to their asymmetric distribution, the degree of carrier accumulation near the positive and negative electrodes in the medium differs [43-44]. Elevated temperatures attenuate the accumulated surface charge, exacerbating the degree of distortion and accelerating the aging process.

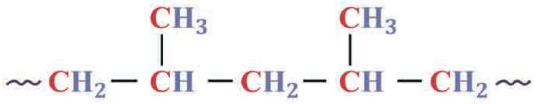

Fig. 14 Molecular structure of PP

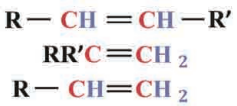

Fig. 15 Types of unsaturated breakage formed by the main chain

3.4.4 Capacitor degradation in alternating humid and thermal environments

The degradation of capacitors in alternating humid and thermal environments is primarily attributed to three aging mechanisms: electrode corrosion, self-healing, and dielectric aging. In contrast to the literatures [6-11], capacitors undergo a relatively rapid decay under high temperatures combined with high humidity, referred to as capacitive aging. During the initial stages of aging in an alternating humid and thermal environment, the capacitor is influenced by the epoxy resin encapsulation and the shell. The onset of aging in the capacitor is dictated by water intrusion into the epoxy resin and its interaction with the metallized electrode and the medium. This is evident from the time required for the capacitor capacity to decay to zero. When the invading water first makes contact with the metal electrode outside the winding structure, the temperature elevation promotes electrode corrosion. The subsequent temperature reduction and low-temperature processes not only encourage capacitor water absorption, but also intensify the proportion and extent of water absorption, thereby accelerating electrode corrosion during the subsequent high-temperature stage in the next cycle. As electrode corrosion progresses, the effective area of the metallized electrode diminishes, the electrode roughness increases, and local breakdown of the dielectric film occurs because of the uneven electric field distribution at the interface and the concentration of space charge. Subsequently, self-healing occurred. In contrast to fixed high-temperature and humidity conditions, the respiratory effect of alternating hot and humid environments fosters the transformation of micropores in the medium itself into larger pores while amplifying the pressure exerted by water on the micropores during dynamic temperature changes, hastening the development of fine cracks. Simultaneously, a higher proportion of water implies more oxygen, leading to complete oxidation in the medium. The short chain resulting from the main-chain break enhances orientation polarization and facilitates film degradation.

4 Life prediction of capacitor

Life prediction was performed by data fitting. C18 in Group 1 was excluded as abnormal data, and the normalized capacity attenuation of each capacitor in Groups 1 and 2 at the same time point is averaged. Owing to their pronounced nonlinearity, the aging characteristic curves of the two capacitor groups are obtained by fitting the data using the $y = A + Be^{Ct}$ provided in Eqs. (7) and (8), where the unit of time is hours. With goodness-of-fit values of 98.86% and 98.76%, respectively, the degree of fit is

notably high.

$$\Delta C_1 = 0.009\,05 - 0.003\,72\exp(0.001\,56t) \quad (7)$$

$$\Delta C_2 = 0.003\,75 - 0.001\,19\exp(0.001\,78t) \quad (8)$$

Fig. 16 shows the capacitance life prediction from 2 232 h to 3 000 h. Tab. 2 presents the calculated life for Groups 1 and 2 under different capacity attenuations, according to Eqs. (7) and (8), respectively. Based on the general definition of the end of life for metallized film capacitors ($-5\%C_0$), the life of Group 1 capacitors is 1 772.2 h, and that of Group 2 is 2 140.7 h. Assuming that the capacitor operates for 12 h per day, the corresponding lifetimes for Groups 1 and 2 are 147.7 d and 178.4 d, respectively. For both groups, a 25% attenuation corresponds to a lifetime of 2 720.1 h (226.7 d) and 3 012.6 h (251 d), while a 50% attenuation corresponds to a lifetime of 3 086.8 h (257.2 d) and 3 339.1 h (278.3 d).

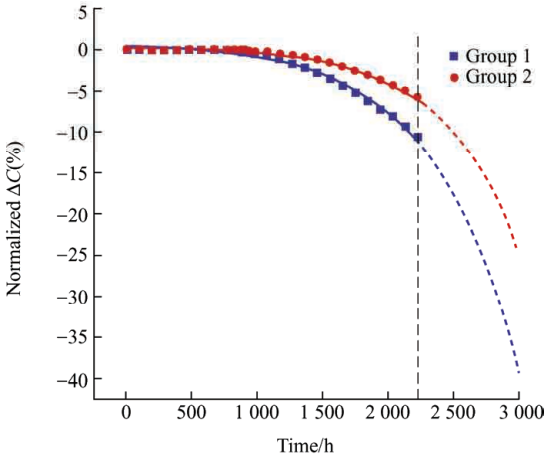

Fig. 16 Life prediction for capacitors in Groups 1 and 2

Tab. 2 Lifetimes corresponding to the different capacitance attenuation of Groups 1 and 2

ΔC(%)	Lifetime/h	
	Group 1	Group 2
5	1 772.2	2 140.7
10	2 165.4	2 510.1
15	2 407.4	2 731.1
20	2 582.6	2 889.3
25	2 720.1	3 012.6
30	2 833.2	3 113.6
35	2 929.3	3 199.2
40	3 012.9	3 273.5
45	3 086.8	3 339.1
50	3 153.1	3 397.8

According to Eqs. (7) and (8), it is evident that parameter C of Group 2 is slightly larger than that of Group 1, which is 1.14 times that of Group 1. This discrepancy may stem from the extended aging time of the DC-link capacitors in Group 2, which is attributed to the more humidity-resistant resin encapsulation. This results in less nonlinear aging data for Group 2 during the same experimental period. However, parameter B of Group 1 is 3.13 times that of Group 2, contributing to a more pronounced nonlinearity in the aging of Group 1 in an alternating humid and thermal environment. In addition to packaging considerations, other crucial factors include ratio of metallized film composition in capacitors, precipitation technology on polypropylene media, and the gap in the "Shoopage" spraying process.

The autocorrelation analysis of the average attenuation of the two groups of normalized capacitors reveals that the autocorrelation function (ACF) of the primary difference between the two groups exhibits a monotonically decreasing tail at an exponential rate. Simultaneously, the partial autocorrelation function (PACF) displays a sinusoidal attenuation truncation, as illustrated in Fig. 17. The ACF of both groups closely

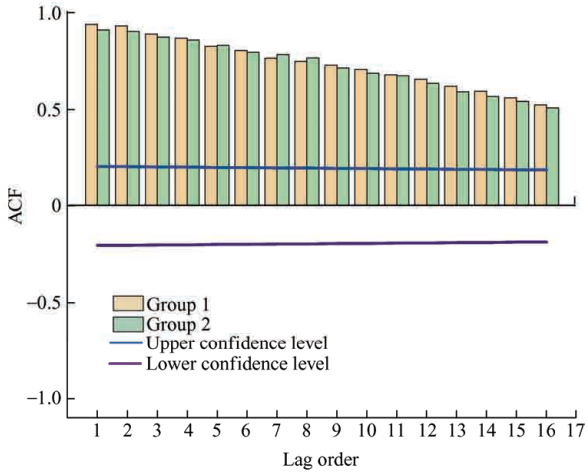

(a) Autocorrelation function

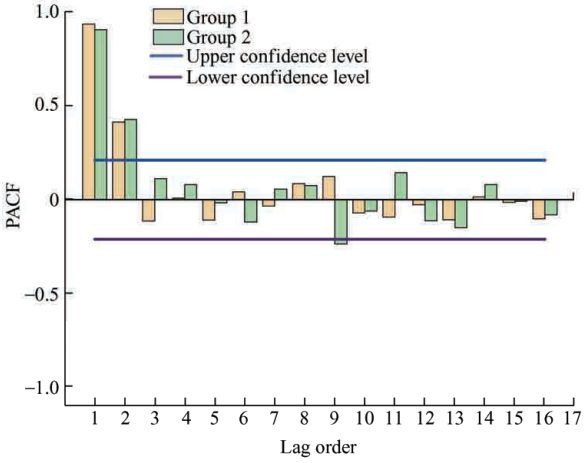

(b) Partial autocorrelation function

Fig. 17 ACF and PACF diagrams of the two sets of capacitors

resemble each other, with the highest correlation observed in the first and second orders. Accordingly, the PACF significantly surpasses the upper and lower limits of confidence, signifying a substantial dependence of the capacitor attenuation at the next moment in the previous two attenuations.

The ultimate empirical life model is influenced by voltage, temperature variations, and humidity. Under specific operational circumstances, the life (L) of the DC-link capacitors with diverse capacity attenuation definitions can be predicted using the following equation

$$\frac{L}{L_N}=\left(\frac{\mathrm{RH}}{\mathrm{RH}_0}\right)^a\left(\frac{V}{V_0}\right)^b 2^{\frac{T_0-T}{c}}\left|\Delta C\right|^d \tag{9}$$

where L_N, RH, RH_0, V, V_0, T_0, T, and ΔC represent the rated life, operating humidity, rated operating humidity, operating voltage, rated voltage, rated temperature, average operating temperature, and normalized capacitance change, respectively. The average operating temperature under alternating humid and thermal conditions is defined as the ratio of the integral area of the temperature curve to the single-cycle time. Correspondingly, the undetermined parameters a, b, c, and d influence these variables. The specific conditions considered in this study are RH=93%, RH_0=60%, V=600 V, and T=45.10. The four undetermined parameters for Group 1 are calculated using Matlab as follows: a_1= –5.607 5, b_1= –5.5, c_1=102.978 8, and d_1=0.195. The corresponding life values for different capacity attenuations are listed in Tab. 2. Additionally, for Group 2, the parameters are determined as a_2= –9.164 7, b_2= –2.563 5, c_2= 6.695 1×10^5, and d_2=0.241 6. Unlike other life models that consider fixed high temperatures and humidity, this model incorporates the average operating temperature in alternating humid and thermal environments. Additionally, it utilizes the change in the normalized capacitance as an independent variable in the model. This unique approach enables prediction of the life of DC-link capacitors under various life definitions.

Fig. 18 displays the fitting curve of the average ESR growth for the capacitances of Groups 1 and 2. Group 1 exhibits a ΔESR of 1.022 at 888 h, whereas Group 2 exhibits a 1.015 ΔESR at 984 h. Group 1 surpasses 3 at approximately 2 000 h of ΔESR, indicating it has reached the end of its life. By the end of the experiment, Group 1 had a 5.044 ΔESR, while Group 2 had 2.705.

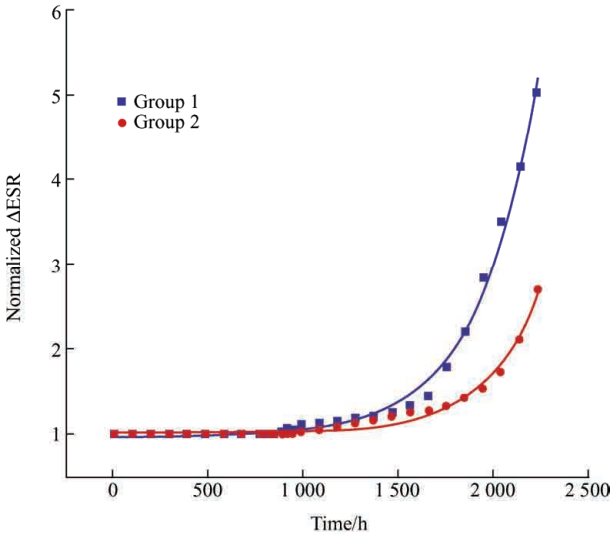

Fig. 18 ESR growth curves for Groups 1 and 2

Similarly, the aging curves of the two groups are obtained by curve fitting the average growth of Groups 1 and 2, leading to the derivation of the growth Eqs. (10) and (11), the goodness of fit is 99.21% and 98.40%, respectively. According to these expressions, the lifetime end points of the two groups of capacitors were calculated, with Groups 1 and 2 having lifetimes of 1 997.8 h (166.5 d) and 2 289.6 h (190.8 d), respectively.

$$\Delta R_1 = 0.966\,4 + 0.003\,76\exp(0.003\,15t) \tag{10}$$

$$\Delta R_2 = 1.013\,85 + 5.599\,07\times10^{-4}\exp(0.003\,57t) \tag{11}$$

5 Conclusions

In this study, 20 metallized polypropylene film capacitors employed in DC-link applications underwent aging in an alternating humid and thermal environment, and an experimental platform was established. This study investigates the aging characteristics of DC-link capacitors, specifically examining their capacity and ESR. The aging mechanism of metallized film capacitors was analyzed from three perspectives: metallized electrode corrosion, self-healing, and overall aging. Capacitor lifetime prediction was conducted through data fitting, and the results indicated the following.

(1) Both the capacity attenuation and ESR increase of the DC-link capacitors demonstrated exponential

nonlinearity under alternating humidity and thermal environments. Considering the life definition of –5% capacity attenuation and 3 times ESR_0, it is evident that capacitance degradation occurs earlier than ESR, reflecting the aging of the capacitor. This observation explains the reason capacity attenuation is widely employed as an aging characteristic in capacitor applications and monitoring.

(2) The time at which the capacitor enters the aging decay phase is influenced by the manufacturing material, process variations of the capacitor itself, and by the packaging material's ability to prevent external moisture ingress. The packaging materials for Groups 1 and 2 are black and white epoxy resins, respectively, as shown in Fig. 4. In the epoxy resin package of Group 1, a curing agent is primarily added to enhance the adhesion, insulation, and antistatic properties. However, the composition and proportion of the curing agent in Group 2 contributed to improved corrosion resistance and heat resistance. The higher maximum operating temperature of Group 2 reflects its superior heat resistance. Regarding water intrusion, the performance disparity in packaging significantly influenced the decay-aging time difference between the two capacitors. In addition, when the winding structures of the two sets of capacitors are similar in volume, a larger volume and package ratio may make water intrusion more challenging and time-consuming.

(3) During the early stage of aging, the gaps between each capacitor in the two groups were not pronounced, and the differences observed in the middle and late stages were attributed to inevitable individual variations, time uncertainties, and measurement errors during the manufacturing process, as well as the influence of contact between capacitors during the aging process. The contact leads to certain portions of the shell obstructing moisture intrusion.

(4) The oxidation and self-healing processes of capacitive metal electrodes reduce their effective areas. Simultaneously, main-chain fracture and crystal transformation of the medium contributed to varying degrees of capacitor aging. During the production of dielectric films, the dielectric properties of polypropylene can be enhanced through long-chain branching modification and by adding various nucleating agents.

References

[1] EMBER. 2022 global electricity review. Britain: EMBER, 2022.

[2] S B Li, X C Li, Y Q Kang, et al. Load capability assessment and enhancement for transformers with integration of large-scale renewable energy: A brief review. *Fontiers in Energy Resarch*, 2022, 10: 1002973.

[3] L C Wang, T Wang, G Huang, et al. Softly collaborated voltage control in PV rich distribution systems with heterogeneous devices. *IEEE Transactions on Power Systems*, 2023, doi: 10.1109/TRWRS. 2023.3347389.

[4] S Y Yang, A Bryant, P Mawby, et al. An industry-based survey of reliability in power electronic converters. *IEEE Transactions on Industry Applications*, 2011, 47(3): 1441-1451.

[5] H Wang, F Blaabjerg. Reliability of capacitors for DC-link applications in power electronic converters: An overview. *IEEE Transactions on Industry Applications*, 2014, 50(5): 3569-3578.

[6] Y Tai, P Chen, Y Jian, et al. Failure mechanism and life estimate of metallized film capacitor under high temperature and humidity. *Microelectronics Reliability*, 2022, 137: 114755.

[7] M Makdessi, A Sari, P Venet. Metallized polymer film capacitors ageing law based on capacitance degradation. *Microelectronics Reliability*, 2014, 54: 1823-1827.

[8] H Li, P Lewin, J C Fothergill. Aging mechanisms of X2 metallized film capacitors in a high temperature and humidity environment. *2016 IEEE International Conference on Dielectrics (ICD)*, 2016, Montpellier, France, 2016: 804-807.

[9] Q R Chen, H Li, L Li, et al. Moisture ingress of metallized film capacitor under high temperature and different humidity condition. *2018 IEEE Conference on Electrical Insulation and Dielectric Phenomena (CEIDP)*, 2018, Cancun, Mexico, 2018: 422-425.

[10] T Qiu, H Li, Z Li, et al. Capacitance loss characteristics of metallized film capacitors under atmospheric corrosion. *2022 IEEE International Conference on High Voltage Engineering and Applications (ICHVE)*, 2022, Chongqing, China, 2022:1-4.

[11] H Wang, D A Nielsen, F Blaabjerg. Degradation testing and failure analysis of DC film capacitors under high humidity conditions. *Microelectronics Reliability*, 2015, 55: 2007-2011.

[12] H B Liu, L Chen, Z Xu, et al. Influence of thermal ageing

on structure and electrical properties of polypropylene film for capacitors. *Insulating Materials*, 2023, 56(2): 96-103.

[13] H Y Li, H Li, Z W Li, et al. Temperature dependence of self-healing characteristics of metallized polypropylene film. *Microelectronics Reliability*, 2015, 55(12): 2721-2726.

[14] N Can, F Aras, V A Alekperov, et al. Investigation on aging mechanism of polyester under combined stresses. *IEEE Electrical Insulation Magazine*, 2016, 32(4): 38-42.

[15] H M Umran, F Wang, Y He. Ageing: Causes and effects on the reliability of polypropylene film used for HVDC capacitor. *IEEE Access*, 2020, 8: 40413-40430.

[16] Y He, F P Wang, G Q Du, et al. Revisiting the thermal ageing on the metallised polypropylene film capacitor: From device to dielectric film. *High Voltage*, 2023, 8(2): 305-314.

[17] Z Y Li, J R Wang, Z Xu, et al. Self-healing characteristics and life prediction of metallized film capacitor under DC voltage. *High Voltage*, 2023, 49(7): 2929-2937.

[18] M Makdessi, A Sari, P Venet, et al. Accelerated ageing of metallized film capacitors under high ripple currents combined with a DC voltage. *IEEE Transactions on Power Electronics*, 2015, 30(5): 2435-2444.

[19] H Li, T Qiu, Z Li, et al. Capacitance loss evolution of Zn-Al metallized film capacitors under atmospheric corrosion. *IEEE Transactions on Dielectrics and Electrical Insulation*, 2022, 29(6): 2363-2369.

[20] Y Tai, P Chen, Y Jian, et al. Failure mechanism and life estimate of metallized film capacitor under high temperature and humidity. *Microelectronics Reliability*, 2022, 137: 114755.

[21] Z Wang, H Li, F Lin, et al. Effects of post-γ irradiation on voltage maintaining performance of high energy density capacitors. *IEEE Transactions on Industry Applications*, 2023, 59(1): 1100-1108.

[22] Chinese People's Liberation Army General Armament Department. GJB 360B-2009 Test methods for electronic and electrical component. Beijing: Chinese People's Liberation Army General Armament Department, 2010.

[23] General Administration of Quality Supervision, Inspection and Quarantine of the People's Republic of China, Standardization Administration of the People's Republic of China. GB/T 2423.4—2016 Environmental testing of electrical and electronic products. Beijing: Standards Press of China, 2016.

[24] IEC 60068-2-30 Environmental Testing-Part 2-30: Tests-Test Db: Damp heat, cyclic(12 h+12 h cycle), IEC/TC125, 2005.

[25] S Boggs, J Ho, T Jow. Overview of laminar dielectric capacitors. *IEEE Electrical Insulation Magazine*, 2010, 26(2): 7-13.

[26] H Li，X Huang, Z W Li, et al. Modeling of ESR in metallized film capacitors and its implication on pulse handling capability. *Microelectronics Reliability*, 2015, 55(7): 1046-1053.

[27] R P Deshpande. Capacitors: Technology and trends. New York: McGraw-Hill, 2012.

[28] R W Brown. Linking corrosion and catastrophic failure in low-power metallized polypropylene capacitors. *IEEE Transactions on Device and Materials Reliability*, 2006, 6(2): 326-333.

[29] H Wang, M Liserre, F Blaabjerg, et al. Transitioning to physics-of-failure as a reliability driver in power electronics. *IEEE Journal of Emerging and Selected Topics in Power Electronics*, 2014, 2(1): 97-114.

[30] N Cabrera, N F Mott. Theory of the oxidation of metals, in world scientific series in 20th century physics. Reports on Progress in Physics, 1995.

[31] S Diaham, M Bechara, M L Locatelli, et al. Dielectric strength of parylene HT. *Journal of Applied Physics*, 2014, 115(5): 054102.

[32] G C Montanari, D Fabiani. Searching for the factors which affect self-healing capacitor degradation under non-sinusoidal voltage. *IEEE Transactions on Dielectrics and Electrical Insulation*, 1999, 6(3): 319-325.

[33] J Kammermaier. Chemical processes during electrical breakdown in an organic dielectric with evaporated thin electrodes. *IEEE Transactions on Electrical Insulation*, 1987, 22(2): 145-149.

[34] J F Zhu, H Tong, J P Luo, et al. Self-healing behaviors of metallized high-temperature dielectric films for capacitor applications. *Microelectronics Reliability*, 2023, 144: 114972.

[35] A Kahouli, O Gallot-Lavallée, P Rain, et al. Structure effect of thin film polypropylene view by dielectric spectroscopy and X-ray diffraction: Application to dry type power capacitors. *Journal of Applied Polymer Science*, 2015, 132(39): 42602.

[36] X Shen, W Hu, T P Russell. Measuring the degree of crystallinity in semicrystalline regioregular Poly (3-hexylthiophene). *Macromolecules*, 2016, 49(12): 4501-4509.

[37] L Capt. Simultaneous biaxial stretching of isotactic polypropylene films in the partly molten state. Montreal: McGill University, 2003.

[38] R A C Deblieck, D J M Van Beek, K Remerie, et al.

Failure mechanisms in polyolefines: The role of crazing, shear yielding and the entanglement network. *Polymer*, 2011, 52(14): 2979-2990.

[39] B Laihonen, J Sari. Polypropylene: Morphology, defects and electrical breakdown. Kemiteknik, 2005.

[40] Z Wang, H Li, F Lin, et al. Effects of post-γ irradiation on voltage maintaining performance of high energy density capacitors. *IEEE Transactions on Industry Applications*, 2023, 59(1): 1100-1108.

[41] M Murzakanova, T Borukaev, M Begretov, et al. The degradation of polyethylene and mechanisms of its stabilisation by azomethinephenylmelamine compounds. *International Polymer Science and Technology*, 2014, 41(11): 43-48.

[42] L A Dissado, C Laurent, G C Montanari, et al. Demonstrating a threshold for trapped space charge accumulation in solid dielectrics under DC field. *IEEE Transactions on Dielectrics and Electrical Insulation*, 2005, 12(3): 612-620.

[43] H Li, L Li, L W Li, et al. Study on the impact of space charge on the lifetime of pulsed capacitors. *IEEE Transactions on Dielectrics and Electrical Insulation*, 2017, 24(3): 1870-1877.

[44] B X Du, W B Zhu, J Li, et al. Temperature-dependent surface charge behavior of polypropylene film under DC and pulse voltages. *IEEE Transactions on Dielectrics and Electrical Insulation*, 2017, 24(2): 774-783.

Quanyi Gao received his B.Sc. degree in Vehicle Engineering from Chongqing University of Technology, Chongqing, China, in 2021. Currently, he is working toward the M.Sc. degree in Electrical Engineering at the School of New Energy and Power Engineering, Lanzhou Jiaotong University. His main research focus is on fault diagnosis and condition monitoring of power equipment.

Shuaibing Li was born in Gansu, China, in 1989. He received the Ph.D. degree in Electrical Engineering in 2018 from Southwest Jiaotong University. Now, he is an Associate Professor with the School of New Energy and Power Engineering, Lanzhou Jiaotong University. His research interests include condition monitoring, assessment and fault diagnosis of high-voltage power equipment, and dynamic state estimation of electrical power systems.

Yi Cui received his B.Eng. and M.Eng. degrees from Southwest Jiaotong University, Chengdu, China, in 2009 and 2012, respectively, and received his Ph.D. degree in Electrical Engineering at the University of Queensland, Brisbane, Australia, in 2016. Dr. Cui has been a Research Fellow in the Department of Electrical Engineering and Computer Science, University of Tennessee, Knoxville in the USA and a Research Fellow at the School of Information Technology and Electrical Engineering, University of Queensland, Australia. Currently, he is a Senior Lecturer in the School of Engineering, University of Southern Queensland, Australia. His research interests include wide-area monitoring and control, data analytics and machine learning of distribution networks, condition assessment and fault diagnosis of power transformers.

Yongqiang Kang was born in Gansu Province, China, in 1988. He received the B.Sc. and M.Sc. degrees in Electrical Engineering from Lanzhou Jiaotong University, Lanzhou, China, in 2008 and 2012, respectively. He received the Ph.D. degree in Electrical Engineering from Southwest Jiaotong University. Now, he is an Associate Professor with the School of New Energy and Power Engineering, Lanzhou Jiaotong University. His research interests include high-voltage asset management, gas discharge and outdoor insulation detection.

Haiying Dong received his Ph.D. degree from Xi'an Jiaotong University in 2003. Now, he is the Dean and a Professor with the School of New Energy and Power Engineering, Lanzhou Jiaotong University. His main research field includes power system optimization and intelligent control, new energy power generation optimization control.